ACS APPLIED MATERIALS & INTERFACES

Research Article

www.acsami.org

Magnesium(II) Bis(trifluoromethane sulfonyl) Imide-Based Electrolytes with Wide Electrochemical Windows for Rechargeable Magnesium Batteries

Se-Young Ha,[†] Yong-Won Lee,[†] Sang Won Woo,[†] Bonjae Koo,[†] Jeom-Soo Kim,[‡] Jaephil Cho,[†] Kyu Tae Lee,*[,†] and Nam-Soon Choi*[,†]

[†]Interdisciplinary School of Energy and Chemical Engineering, Ulsan National Institute of Science and Technology (UNIST), 100 Banyeon-ri, Eonyang-eup, Ulju-gun, Ulsan 689-798, South Korea

[‡]Department of Chemical Engineering, Dong-A University, 840 Hadan2 dong, Saha-gu, Busan, South Korea

Supporting Information

ABSTRACT: We present a promising electrolyte candidate, $Mg(TFSI)_2$ dissolved in glyme/diglyme, for future design of advanced magnesium (Mg) batteries. This electrolyte shows high anodic stability on an aluminum current collector and allows Mg stripping at the Mg electrode and Mg deposition on the stainless steel or the copper electrode. It is clearly shown that nondendritic and agglomerated Mg secondary particles composed of ca. 50 nm primary particles alleviating safety concern are formed in glyme/diglyme with 0.3 M $Mg(TFSI)_2$ at a high rate of 1C. Moreover, a $Mg(TFSI)_2$-based electrolyte presents the compatibility toward a Chevrel phase Mo_6S_8, a radical polymer charged up to a high voltage of 3.4 V versus Mg/Mg^{2+} and a carbon−sulfur composite as cathodes.

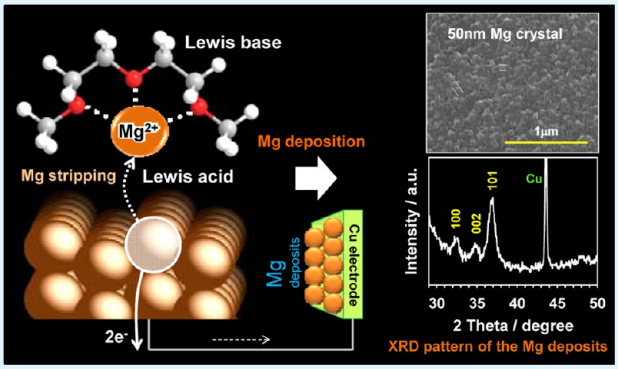

KEYWORDS: *electrochemistry, diglyme, magnesium battery, magnesium deposition, magnesium stripping*

1. INTRODUCTION

The need for inexpensive and safe rechargeable batteries for large-scale environmentally benign cells has intensified in recent years, with the emergence of uses such as energy storage systems for large-scale applications, electric vehicles, and various types of portable electronic devices.[1−4] Magnesium batteries have recently gained recognition as a promising candidate for next-generation battery systems, largely on the basis of the high volumetric capacity, high specific capacity (3832 mAh/cm^3 and 2230 mAh/g), and low reduction potential (−2.356 V versus standard hydrogen electrode) of Mg metal and the natural abundance of Mg resources.[5−13] The development of magnesium electrolytes is considered the most important challenge for the commercial application of rechargeable magnesium (Mg) batteries because electrolyte properties govern battery performance and determine the class of cathodes utilized.[11] It has been reported that the Mg electrode shows highly reversible behavior and that Mg batteries present superior cycling properties among a family of electrolyte solutions based on organohaloaluminate Mg salts in tetrahydrofuran (THF) developed by the Aurbach group.[14] The tri(3,5-dimethylphenyl)borane (Mes_3B)-$(PhMgCl)_2$ electrolyte, formed through the reaction of Mes_3B and PhMgCl in THF, was found to yield outstanding electrochemical performance for Mg/Mo_6S_8.[15] Very recently, it was reported that a halide-free inorganic salt, magnesium borohydride $Mg(BH_4)_2$, with $LiBH_4$ showed unprecedented reversible Mg deposition and stripping in dimethoxyethane (glyme) solvents.[12] Mg deposition and stripping are very difficult in most nonaqueous organic electrolytes based on $Mg(ClO_4)_2$ because the surface species that form on Mg electrodes are electronically insulating (which leads to passivation of the electrode) and do not assist the migration of Mg ions to the Mg electrode surface.[16] It is therefore very important to find suitable electrolytes for rechargeable Mg batteries. To this end, reversible Mg deposition and stripping, high ionic conductivity, and wide electrochemical windows must be attained. In this regard, the Aurbach group reported an inorganic magnesium salt solution synthesized by the acid−base reaction of $MgCl_2$ and Lewis acidic compounds such as $AlCl_3$. This electrolyte showed upward of 99% Coulombic efficiency, low overpotential (<200 mV) for Mg deposition, and good anodic stability of 3.1 V Mg/Mg^{2+}.[17] In addition, there is strong demand for the development of electrolyte systems with low air/moisture sensitivity and low volatility to ensure battery safety. The Liao group presented a synthetic strategy to enhance the oxidation stability of oxygenated species of modified Grignard reagents by replacing phenolate with alkoxides while maintaining their

Received: December 6, 2013
Accepted: February 21, 2014
Published: February 21, 2014

Table 1. Physical Properties of Cyclic and Linear Ether Solvents

Solvent	Chemical structure	Donor number (kcal/mol)	Boiling point (°C)
AN [a]		14.1	81
THF [b]		20.0	66
Glyme [c]	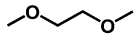	24.0	85
Diglyme [d]	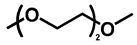	19.5	162
Triglyme [e]	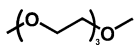	-	216
Tetraglyme [f]	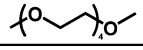	16.6	275

[a]Acetonitrile. [b]Tetrahydrofuran. [c]Dimethoxy ethane. [d]Diethyleneglycol dimethyl ether. [e]Triethyleneglycol dimethyl ether. [f]Tetraethyleneglycol dimethyl ether.

favorable air/moisture stable features.[18] Mg/Mo_6S_8 batteries in complexes of alkoxide-based magnesium salts with the Lewis acid $AlCl_3$ at a ratio of 1:6 ($AlCl_3$:ROMgCl) displayed good cycling and rate performance at both 20 and 50 °C. the electrochemical magnesiation and demagnesiation of an Mg_2Sn anode coupled with a Chevrel phase (Mo_6S_8) cathode were reported for $Mg(TFSI)_2$ dissolved in a highly volatile glyme solvent with a low boiling temperature of 85 °C.[19] The Obrovac group reported the very interesting results that an acetonitrile (AN) solvent reduces on the anode at a low voltage of approximately −1.2 V versus Mg/Mg^{2+} at 60 °C.[20]

Herein, we propose a new class of electrolytes based on magnesium(II) bis(trifluoromethane sulfonyl)imide ($Mg[N(SO_2CF_3)_2]_2$), $Mg(TFSI)_2$) dissolved in glyme-based solvents with unique characteristics such as a highly reduced corrosive nature toward the current collector, a high anodic limit, low volatility, high solvating power, and the ability to form an appropriate solvation sheath structure for Mg stripping/deposition. Because a high dielectric constant and low viscosity usually cannot be integrated into a single solvent, a solvent mixture, usually binary with one of the components selected for solvating power and the other for viscosity, is used to formulate the electrolytes for Li batteries. Similarly, an appropriate electrolyte formulation for Mg batteries should be identified to enhance ionic conductivity, the stabilization of electrodes, cell performance, and safety. This approach is a simple and effective way to allow reversible Mg stripping/deposition, which has not been previously reported. Moreover, the unique properties of glyme-based electrolytes in Mg/Mo_6S_8, Mg/poly(2,2,6,6-tetramethyl-piperidinyl-1-oxy-4-yl methacrylate) (PTMA), and Mg/CMK3-S cells are discussed.

2. EXPERIMENTAL SECTION

2.1. Materials. All tested electrolytes consisted of a magnesium bis(trifluoromethane sulfonyl)imide ($Mg(TFSI)_2$) (492 ppm of moisture, Kishida Chemical Co. Ltd.) in tetrahydrofuran (THF, 24 ppm of moisture, Aldrich, anhydrous, 99.9%), dimethoxyethane (glyme, 57 ppm of moisture, Aldrich, anhydrous, 99.9%), diethylene glycol dimethyl ether (diglyme, 52 ppm of moisture, Aldrich, anhydrous, 99.5%), triethylene glycol dimethyl ether (triglyme, 63 ppm of moisture, Aldrich, 99.0%), tetra(ethylene glycol dimethyl ether (tetraglyme, 89 ppm of moisture, Aldrich, >99.0%) or binary solvent mixtures (glyme/diglyme = 50/50 vol%). Solvents were used as received. A solution of 0.5 M $AlCl_3$ in THF (Aldrich, 99.9%) was slowly added dropwise to a predetermined quantity of 2 M phenylmagnesiumchloride (PhMgCl)/THF solution (Aldrich). The resulting solution, 0.4 M $(PhMgCl)_2$-$AlCl_3$ in THF, was stirred for an additional 16 h at room temperature.[21] The bulk electrolyte used for the electrochemical tests of Mg/PTMA and Mg/CMK3-S cells was 0.3 M magnesium bis(trifluoromethane sulfonyl)imide ($Mg(TFSI)_2$) dissolved in binary ether solvents of glyme/diglyme (1/1, v/v) (48 ppm of moisture). The effects of various solvents, such as acetonitrile (AN, 5.7 ppm of moisture Aldrich, anhydrous, 99.8%), THF, tetraglyme, triglyme, diglyme, and glyme on Mg stripping from the Mg electrode were tested. All the solvents were purchased from Aldrich. The chemical structure and physical properties of each solvent are listed in Table 1.

2.2. Characterization. The attenuated total reflectance−Fourier transform infrared (ATR-FTIR) spectra of the electrolytes were recorded by reflectance measurements obtained using a Varian 670-IR spectrometer with a spectral resolution of 4 cm^{-1} under a nitrogen atmosphere. Scanning electron microscope (SEM; JEOL JSM-6700F) images and EDS spectra of pristine and cycled Mg electrodes were recorded using an FEI Nanonova 230 with a field emission gun and energy-dispersive X-ray spectroscopy (EDS) detector. The cycled cells were disassembled in an argon filled glovebox, and the Mg electrodes retrieved from the disassembled cells were immersed in distilled THF and shaken for 30 s to remove excess surface bound electrolyte, then sealed in pouches for transport to the SEM. The galvanostatically deposited Mg on a Cu electrode was characterized via X-ray diffraction (XRD) operated from 2θ = 10−80° at a rate of 1 degree per minute using monochromatic Cu Kα radiation. The ionic conductivity of the electrolytes was measured using an Oakton CON 11 standard conductivity meter at room temperature. The oxidative stability of the electrolytes was evaluated in two-electrode coin cells using a magnesium metal disc (thickness = 1000 μm, GoodFellow, 99.9%) as the counter and reference electrodes and stainless steel (SS, SUS316L, 1.77 cm^2) as the working electrode. Scanning electron microscope (SEM; JEOL JSM-6700F) images and EDS spectra of pristine and cycled Mg electrodes were recorded using an FEI Nanonova 230 with a field emission gun and an energy-dispersive X-ray spectroscopy (EDS) detector.

2.3. Electrochemical Tests. The anodic limits of the electrolytes were determined by linear sweep voltammetry (LSV) using an Iviumstat (Ivium Technologies, The Netherlands). We used 2-electrode cells with SS as the working electrode and disc-type Mg electrode as the reference and counter electrodes. The magnesium electrodes were thoroughly polished three times with sandpaper to remove the oxide layer of such species as MgO and/or $Mg(OH)_2$, then rinsed with dry THF distilled with a sodium-benzophenone complex prior to use. The polished Mg electrodes were utilized within 5 s to make cells in a glovebox used only for Mg batteries to minimize any possible oxidation of the Mg surface (see Figure S1 in the Supporting Information). For electrochemical tests of the Mg/Mg and Mg/Cu cells, coin-type cells with a Mg (or Cu) working electrode and a Mg metal counter electrode were assembled in an argon filled glovebox

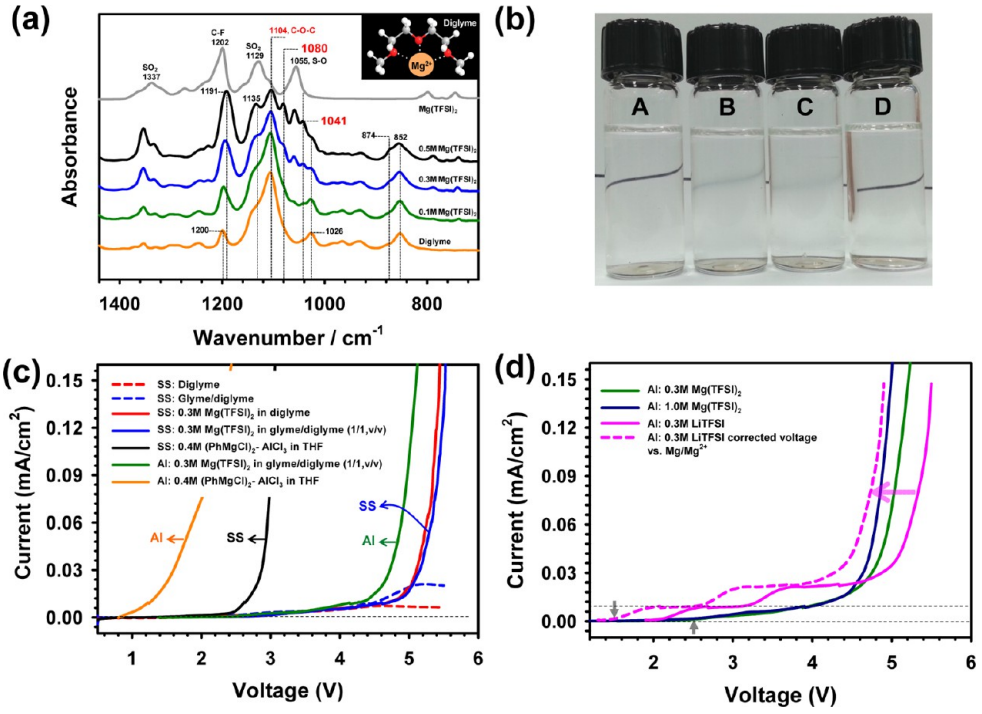

Figure 1. (a) FT-IR spectra of diglyme solvent, 0.1, 0.3, and 0.5 M $Mg(TFSI)_2$ dissolved in diglyme, and $Mg(TFSI)_2$ salt. The inset shows a schematic drawing of the ion-dipole interaction between Mg^{2+} ions and diglyme solvent. (b) Photo showing the solubility limit of $Mg(TFSI)_2$ in glyme or glyme/diglyme mixed solvent: (A) pure glyme, (B) glyme with 0.1 M $Mg(TFSI)_2$, (C) glyme with 0.3 M $Mg(TFSI)_2$,(D) glyme/diglyme with 0.3 M $Mg(TFSI)_2$ at room temperature. (c) Linear sweep voltammetry of various electrolytes and solvents. Stainless steel (SS) or aluminum (Al) was used as a working electrode, and the scanning rate was 20 mV/s. (d) Linear sweep voltammetry (LSV) of LiTFSI and $Mg(TFSI)_2$ in glyme/diglyme (1/1, v/v) on an Al electrode at a scan rate of 20 mV/s. The potential scan was initially conducted in the anodic direction from open circuit voltage (OCV → 5.5 V vs Mg). LSV data obtained from 0.3 M LiTFSI in glyme/diglyme (1/1, v/v) were corrected as −0.6 V. The voltage of Mg electrode versus Li or SHE is shown in Figure S3 in the Supporting Information.

with less than 1 ppm of both oxygen and moisture. The cycling experiments for Mg/Cu (2016 coin-type) and Mg/Mg (2032 coin-type) cells were galvanostatically conducted using a computer-controlled battery measurement system (WonATech WBCS 3000). The Mo_6S_8 cathode material was synthesized according to a procedure reported in the literature.[22] The Mo_6S_8 composite cathode was prepared by casting and pressing a 7:2:1 weight-ratio mixture of Mo_6S_8, super-P carbon powder, and poly(vinylidene fluoride) (PVDF) binder on a SS foil. Poly(2,2,6,6-tetramethyl-piperidinyloxy-4-yl methacrylate) (PTMA) cathode material was synthesized according to a procedure reported in the literature.[23] The PTMA composite cathode was prepared by casting and pressing a 4:5:1 weight-ratio mixture of PTMA, super-P carbon, and PVDF binder on aluminum (Al) foil. The CMK-3/sulfur (S) nanocomposite was prepared following a melt-diffusion strategy.[24] The cathodes were composed of a 70 wt % CMK-3/S composite, 20 wt % super-P carbon, and 10 wt % PVDF binder. The cathode was slurry-cast onto an aluminum current collector. A coin-type cell (2032) was used for full-cell tests, and microporous polyethylene film was used as a separator.

3. RESULTS AND DISCUSSION

3.1. Oxidation Stability of $Mg(TFSI)_2$-Based Electrolytes. The solvation of Mg^{2+} ions via ion-dipole interaction can be improved by the use of glymes with oxygen atoms showing high electron donicity. To clarify the influence of a family of glyme-based solvents on coordination with Mg^{2+} ions, Fourier-transform infrared (FT-IR) analyses were performed. If an interaction occurs in a material, a peak corresponding to a specific functional group in the FT-IR spectrum shifts toward either a higher or lower wavenumber, or a new peak (or shoulder) appears in the spectrum. Figure 1a shows a clear disparity between pure diglyme solvent and diglyme with $Mg(TFSI)_2$ salt in the frequency regions characteristic of C−O−C and C−C coupled with C−O stretching. A new peak at 1080 cm^{-1} in the C−O−C region was produced by the addition of $Mg(TFSI)_2$ salt to a diglyme solvent, and the peak intensity gradually increased as a function of salt concentration (Figure 1a). This result is persuasive evidence that diglyme with a high donor number of 19.5 kcal/mol solvates Mg^{2+} ions sufficiently to prevent ion pairing (inset of Figure 1a, Table 1). A pronounced new peak in the frequency region, which is characteristic of C−C stretching vibration coupled with the C−O stretching of a diglyme solvent, appeared at 1041 cm^{-1} due to the introduction of $Mg(TFSI)_2$ salt. This result implies that the ion-dipole interaction between the ether moiety and the Mg^{2+} ions affects the C−C stretching vibration mode. The characteristic band of the CH_2 rocking vibration coupled with C−O stretching is located at 852 cm^{-1}. In this region, a new shoulder peak, which arises from coordination between the C−O group and the Mg^{2+} ions, is clearly seen at 874 cm^{-1}. Although glyme has a 24 kcal/mol higher donor number than diglyme, as shown in Table 1, $Mg(TFSI)_2$ salt in a concentration exceeding 0.1 M does not easily dissolve in the glyme solvent. Figure 1b shows that $Mg(TFSI)_2$ partially breaks up into charged ions in glyme; its solution is consequently semitransparent. Moreover, two separated layers were observed in a 0.3 M solution of $Mg(TFSI)_2$ in glyme. This result indicates that the organic solvent should not only have high solvating power but should also form a stable solvation sheath structure based on ion-dipole interaction to dissociate the highly concentrated Mg salt. Similarly, $Mg(TFSI)_2$ salt in a

dx.doi.org/10.1021/am405619v | ACS Appl. Mater. Interfaces 2014, 6, 4063−4073

concentration exceeding 0.1 M did not dissolve in the THF solvent. A new peak at 875 cm^{-1} in the C−O−C region was produced by the addition of $Mg(TFSI)_2$ salt to THF, and the peak intensity increased slightly as a function of salt concentration (see Figure S2a in the Supporting Information). This result is likely because of the low dissociation degree of $Mg(TFSI)_2$ salt in THF. Indeed, in the case of THF-based electrolytes, the peak corresponding to $Mg(TFSI)_2$ salt, which was not observed in diglyme/0.3 M $Mg(TFSI)_2$ electrolyte, appeared at approximately 1630 cm^{-1} (see Figure S2b in the Supporting Information).

Figure 1c presents typical linear sweep voltammetry (LSV) curves for various electrolytes and solvents. Stainless steel (SS), an important component in testing coin cells, was used as a working electrode. A solution of 0.4 M $(PhMgCl)_2$-$AlCl_3$/THF, which is the magnesium organohaloaluminate electrolyte, displays an electrochemical stability window of up to 2.5 V versus a Mg reference electrode on a SS working electrode. The oxidative stability of electrolytes based on ether solvents and $Mg(TFSI)_2$ on an SS working electrode was investigated. Interestingly, $Mg(TFSI)_2$ dissolved in diglyme or glyme/diglyme showed no appreciable anodic current up to 3.0 V and a slight increase of the anodic current at approximately 3.0 V on a SS electrode (Figure 1c, d). The LSV result of glyme/diglyme with 0.3 and 1.0 M $Mg(TFSI)_2$ on an aluminum (Al) working electrode suggests that the oxidation current attributed to Al corrosion was not induced up to 2.5 V versus Mg/Mg^{2+}. Although the anodic current began to increase at 3.0 V, there was no significant current even at 4.0 V (Figure 1c,d). However, after increasing the anodic current at 1.5 V versus Mg/Mg^{2+}, 0.3 M LiTFSI in glyme/diglyme (1/1, v/v) exhibited a steadily increasing oxidation current and eventually produced considerable current on an Al electrode (Figure 1d). This result indicates that the extent of Al corrosion is greatly reduced in $Mg(TFSI)_2$-based electrolytes compared with the LiTFSI-based electrolyte. Very recently, the Balducci group proposed that $Al(TFSI)_3$ formed by the reaction of the Al surface with TFSI anions is minimally soluble in TFSI-based ionic liquid, and thereby the Al corrosion was profoundly suppressed.[25] If Al-TFSI complexes are readily soluble in the electrolyte, severe Al corrosion should take place continuously. The importance of the solubility of Al-TFSI complexes in the electrolyte appears to be a very rational explanation. The formed $Al(TFSI)_3$ may be minimally soluble in Mg(TFSI)-based electrolyte and act as a passivation layer mitigating the Al corrosion. At the same salt concentration, the concentration of TFSI anions generated from $Mg(TFSI)_2$ is twice as high as with LiTFSI in the electrolyte. This high charge carrier concentration in the $Mg(TFSI)_2$-containing electrolyte will reduce the solubility of Al-TFSI complexes, and thereby the Al corrosion will be mitigated even in the presence of TFSI anions. This speculation is reasonable because $Mg(TFSI)_2$ salt in a concentration exceeding 1.0 M does not dissolve in glyme/diglyme, as shown in Table 2.

It should be noted that Al is not stable beyond 1.2 V with $Mg(AlCl_2EtBu)_2$/THF and $AlCl_3$-$(PhMgCl)_2$/THF electrolytes.[15] Similarly, the 0.4 M $(PhMgCl)_2$-$AlCl_3$/THF electrolyte began to oxidize at a low voltage of 1.0 V (Figure 1c). the Aurbach group reported that the use of carbonaceous current collectors leads to impressively prolonged cycling of Mg/Mo_6S_8 cells with the second generation electrolyte Mg organohaloaluminate complex.[6] $Mg(TFSI)_2$/glyme/diglyme conventional electrolytes can potentially be good candidates, which would make the use of commercial current collectors such as Al and SS possible. Pure glyme and diglyme solvents did not generate anodic current on the SS working electrode, as shown in Figure 1c, most likely because the passivation layer formed on an SS working electrode by the anodic reactions of a pure solvent without salt makes further anodic decomposition more difficult. We speculate that the inherent thermodynamic anodic instability of Mg salt in the electrolyte solution does not produce a suitable passivation layer to inhibit the oxidative decomposition of the electrolyte.[26] A solution of 0.3 M $Mg(TFSI)_2$ in glyme/diglyme (1/1, v/v) showed potential stability up to 4.0 V at a low scan rate of 0.2 mV/s, which was applied to exclude the effects of polarization resistance on the anodic limit (Figure 2). This preliminary evidence suggests that $Mg(TFSI)_2$ dissolved in ether-based solvents lessens the corrosion nature of an electrolyte and would enable rechargeable magnesium batteries to be operated over 2 V versus Mg/Mg^{2+}. To understand the effects of solvent species on Mg stripping/deposition, we investigated the potential behaviors of various solvents with 0.1 M $Mg(TFSI)_2$.

Table 2. Ionic Conductivities of Electrolytes

solvents	salt	ion conductivity (S cm^{-1})
glyme	0.1 M $Mg(TFSI)_2$	0.54×10^{-3}
diglyme	0.3 M $Mg(TFSI)_2$	2.52×10^{-3}
glyme/diglyme (1/1, v/v)	0.1 M $Mg(TFSI)_2$	0.58×10^{-3}
glyme/diglyme (1/1, v/v)	0.3 M $Mg(TFSI)_2$	3.03×10^{-3}
glyme/diglyme (1/1, v/v)	0.5 M $Mg(TFSI)_2$	5.22×10^{-3}
glyme/diglyme (1/1, v/v)	1.0 M $Mg(TFSI)_2$	4.31×10^{-3}
glyme/diglyme (1/1, v/v)	1.3 M $Mg(TFSI)_2$	not measurable because of the insolubility of salt
dichloro complex solutions,[6] which are the products of the reaction between 1 equiv. of Bu_2Mg with 2 equiv. of $EtAlCl_2$		$1-1.4 \times 10^{-3}$

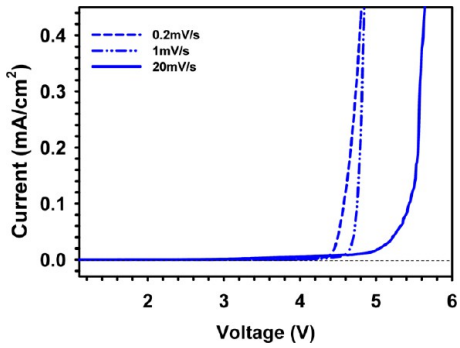

Figure 2. Linear sweep voltammetry of glyme/diglyme (1/1, v/v) with 0.3 M $Mg(TFSI)_2$ on a SS electrode at different scan rates.

It is worth pointing out that a freshly prepared Mg electrode is covered by an insulating oxide layer such as MgO and/or $Mg(OH)_2$.[6] This oxide layer will lead to voltage delay for the first Mg stripping from the Mg electrode.

3.2. Mg Stripping and Deposition in $Mg(TFSI)_2$-Based Electrolytes. Figure 3a presents the voltage profiles for Mg/Cu cells for the current density of 0.081 mA/cm^2 (corresponding capacity = 3.25 mAh/cm^2). Interestingly, the

dx.doi.org/10.1021/am405619v | ACS Appl. Mater. Interfaces 2014, 6, 4063−4073

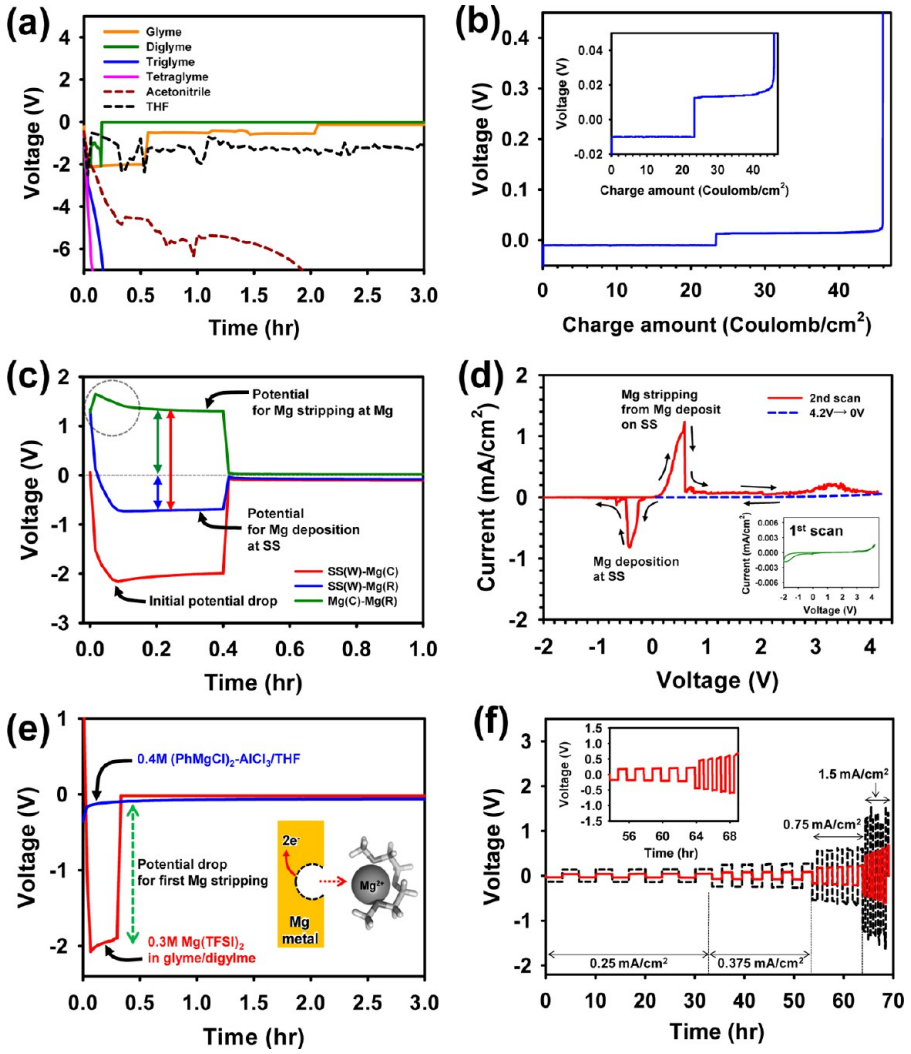

Figure 3. (a) Relation between the initial overpotential of Mg/Cu cells and electrolytes with 0.1 M $Mg(TFSI)_2$ for the current density of 0.0188 mA/cm^2. (b) Voltage profiles of a Mg/SS cell in glyme/diglyme (1/1, v/v) with 0.3 M $Mg(TFSI)_2$ for a fixed charge amount of 23.4 coulomb/cm^2 (0.325 mA/cm^2). (c) Voltage profiles of a SS/Mg/Mg cell (three-electrode cell) with 0.3 M $Mg(TFSI)_2$ in glyme/diglyme (1/1, v/v) at 30 °C. W, working electrode; C, counter electrode; R, reference electrode. (d) Cyclic voltammetry showing Mg deposition/stripping on a SS electrode in 0.3 M $Mg(TFSI)_2$ in glyme/diglyme (1/1, v/v) at a scan rate of 0.2 mV/s. (e) Initial potential drop of Mg/Cu cells in 0.4 M $(PhMgCl)_2$-$AlCl_3$/THF (blue line) or glyme/diglyme (1/1, v/v) with 0.3 M $Mg(TFSI)_2$ (red line) for the current density of 0.1625 mA/cm^2. The inset shows a schematic illustration of Mg stripping by diglyme forming a stable solvation sheath. (f) Rate capability of Mg/Mg cells with 0.3 M $Mg(TFSI)_2$ in glyme/diglyme (1/1, v/v) (red line) or diglyme (dashed black line) for current densities of 0.25, 0.375, 0.75, and 1.5 mA/cm^2. The inset displays potential profiles for the current densities of 0.75 and 1.5 mA/cm^2.

acetonitrile (AN) solvent exhibited an initial steep overpotential, indicating very difficult initiation of Mg stripping/deposition, and the potential was significantly decreased to −10 V during the further cathodic direction scan. This result is in good agreement with a previous finding that AN reductive decomposition occurs instead of Mg stripping/deposition at low negative voltages.[20]

Note that the cyclic ether solvent THF with 0.1 M $Mg(TFSI)_2$ showed a greatly reduced potential barrier for Mg stripping/deposition during the first cathodic scan compared to the AN solvent (Figure 3a), but an overpotential of approximately 1 V did not disappear during the further cathodic scan. A greater overpotential of Mg/Cu cells was observed in 0.1 M $Mg(TFSI)_2$ in glyme at the initial stages of the first cathodic scan, and the potential thereafter shifted toward −13 mV (Figure 3a). This result indicates that glyme/0.1 M $Mg(TFSI)_2$ eliminates the oxide layer on the Mg electrode at the beginning of the cathodic scan, and therefore Mg stripping from the Mg electrode and Mg deposition at the Cu electrode readily take place in a glyme solvent. Nevertheless, a large overpotential was still observed for 2 h. To enhance the practical application of the electrolytes and reduce overpotential for the first Mg stripping/deposition during first cathodic scan, weconsidered a diglyme solvent with a high boiling temperature of 162 °C and a high donor number (D.N. = 19.5 kcal/mol), indicating high solvating power toward Mg.

Similarly, a large overpotential was apparent at the beginning of the first Mg stripping from the Mg electrode in diglyme with 0.1 M $Mg(TFSI)_2$. The overpotential then almost disappeared after only 10 min, and a potential of around −15 mV, indicating very low ohmic resistance for Mg stripping from the Mg electrode and Mg deposition at the Cu electrode, was maintained at the end of the first cathodic direction scan. The voltage delay region of diglyme (DN=19.5 kcal/mol)/0.1

dx.doi.org/10.1021/am405619v | ACS Appl. Mater. Interfaces 2014, 6, 4063−4073

M $Mg(TFSI)_2$ was shorter than for glyme (DN = 24.0 kcal/mol)/0.1 M $Mg(TFSI)_2$ during the first Mg stripping/deposition. In the case of triglyme and tetraglyme solvents, which have long ether chains, an extremely large overpotential appeared, as seen in Figure 3a. This result is likely because the solvating power of tetraglyme (D.N. = 16.6 kcal/mol) is not sufficient to remove the oxide layer on the initial surface of Mg electrode under an electric field (Table 1).[27] Indeed, the introduction of a glyme solvent could slightly improve the ionic conductivity of an electrolyte (Table 2). therefore, a glyme/diglyme (1/1, v/v) mixture was considered as a solvent for an electrolyte. Note that 0.3 M $Mg(TFSI)_2$ in a glyme/diglyme mixed solvent exhibited the lowest potential barrier at the beginning of the first cathodic scan (Figure 4a). A salt concentration of 0.5 M in a glyme/diglyme mixed solvent led to a large potential drop between the two Mg electrodes, and this

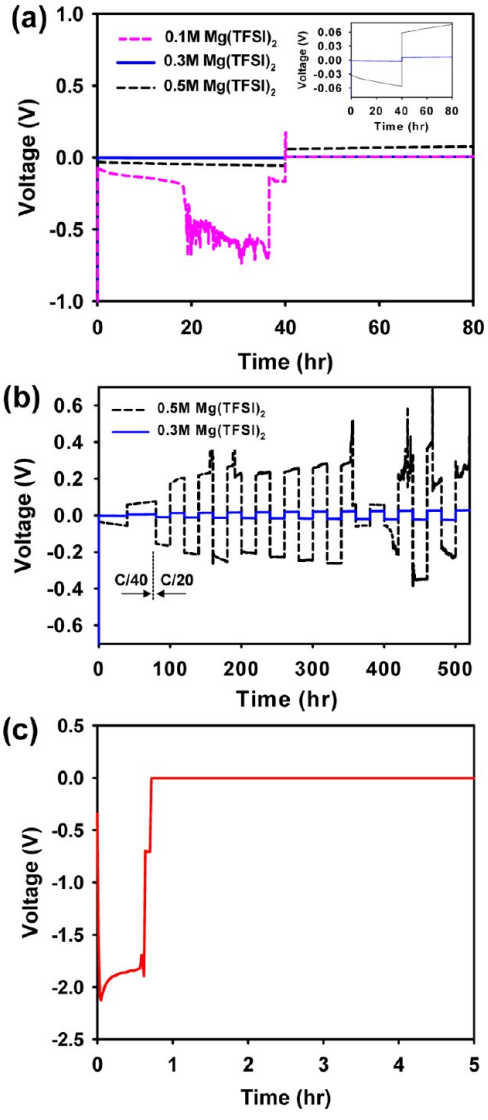

Figure 4. (a) Overpotential profiles of Mg/Mg cells in glyme/diglyme (1/1, v/v) with various $Mg(TFSI)_2$ concentrations, (b) galvanostatic cycling of Mg/Mg cells at a rate of *C*/20 after the first cycle at *C*/40, and (c) enlarged region showing the initial overpotential of a Mg/Cu cell in glyme/diglyme (1/1, v/v) with 0.3 M $Mg(TFSI)_2$ at a rate of *C*/20. A current density of 0.0188 mA/cm^2 (corresponding to a rate of *C*/40) was applied to the Mg/Mg and Mg/Cu cells.

overpotential increased with an increase in the applied current from 0.0188 mA/cm^2 to 0.0375 mA/cm^2 (corresponding capacity = 0.75 mAh/cm^2) (Figure 4b). Although 0.5 M $Mg(TFSI)_2$ in glyme/diglyme has a high ionic conductivity of 5.22×10^{-3} S/cm (Table 2), high potential barriers and unstable potential profiles for the Mg stripping and deposition processes were observed during cycling. This result suggests that most solvents contribute to the dissociation of 0.5 M $Mg(TFSI)_2$, the fraction of free solvent, which can dissociate. The more ions that exist in the electrolyte, the higher the ionic conductivity. However, after the highest ionic conductivity is reached at 0.5 M $Mg(TFSI)_2$ in glyme/diglyme, the ionic conductivity drops. This result is likely because of the presence of undissociated salt retarding the movement of free ions in the electrolyte and the increase in electrolyte viscosity with increasing $Mg(TFSI)_2$ concentration. During the first cathodic direction scan, Mg deposition occurred on the SS electrode, while Mg was stripped from the Mg counter electrode (Figure 3b).

A solution of 0.3 M $Mg(TFSI)_2$ in glyme/diglyme showed an overpotential of approximately −2.0 V versus Mg/Mg^{2+}, which is similar to glyme and diglyme-based electrolytes, and then rapidly increased to approximately −10 mV (Figure 3b and Figure 4c). This result indicates that the activation process is required for Mg stripping from the Mg electrode and Mg deposition on the Cu electrode in 0.3 M $Mg(TFSI)_2$ dissolved in a glyme/diglyme mixed solvent. This potential drop disappeared after 42 min (Figure 4c). It is clearly seen that many holes on the surface of the Mg electrode were produced during the first cathodic scan, and their morphology was quite similar to the holes obtained from THF, glyme, diglyme, and glyme/diglyme-based electrolytes (Figure 5, see Figure S4 in the Supporting Information). After the first cathodic direction scan (Mg deposition of 23.4 Coulomb/cm^2, current density = 0.325 mA/cm^2), Mg stripping of 22.5 Coulomb/cm^2 took place from the Mg deposits on the SS electrode, while Mg was deposited on the Mg counter electrode (Figure 3b). High Coulombic efficiency of 96.1% was achieved for the initial Mg deposition/stripping process. No large overpotential for Mg stripping from the Mg deposits on the SS electrode was observed. This result appears to be caused by the different morphology between the deposited Mg particles and the pristine Mg metal. To confirm the origin of the initial overpotential of Figure 3b, the voltage curves of a three-electrode cell with a SS working electrode, a Mg reference electrode, and a Mg counter electrodes were monitored (Figure 3c). It can be clearly seen that the overpotential for the first Mg stripping from the Mg electrode was much higher than for the Mg deposition on a SS electrode. This result indicates that the initial overpotential can be largely ascribed to the overpotential for Mg stripping. Although no Mg deposition/stripping occurred during the first scan, highly reversible Mg deposition/stripping were observed during the second scan (Figure 3d). In the second negative scan, a reduction peak appeared at −0.4 V, which is attributed to Mg deposition on the SS electrode. During the following positive scan, an oxidation peak corresponding to Mg stripping was observed at 0.5 V. After a slight increase in the anodic current at 2.9 V in glyme/diglyme with 0.3 M $Mg(TFSI)_2$, the current decreased at around 4.2 V without appreciable oxidation current. In the third scan, there was no further improvement for Mg deposition/stripping (see Figure S5 in the Supporting Information). The 0.4 M $(PhMgCl)_2$-$AlCl_3$/THF electrolyte

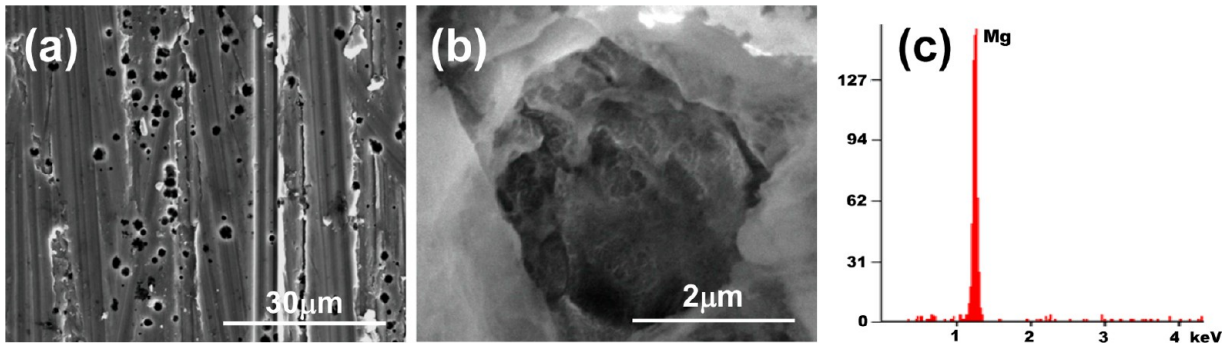

Figure 5. SEM images and EDS spectra for Mg electrodes after first Mg stripping (corresponding capacity = 3.25 mAh/cm^2) in 0.1 M Mg(TFSI)$_2$ dissolved in glyme/diglyme (1/1, v/v). (a, b) The SEM images reveal that all Mg electrodes after the first Mg stripping (3.25 mAh/cm^2) at a rate of C/40 had nonuniform micropores, and their surface morphology was analogous. (c) Importantly, only a pronounced Mg signal for all Mg electrodes was detected without other elements (C and O), which can be produced by electrolyte decomposition.

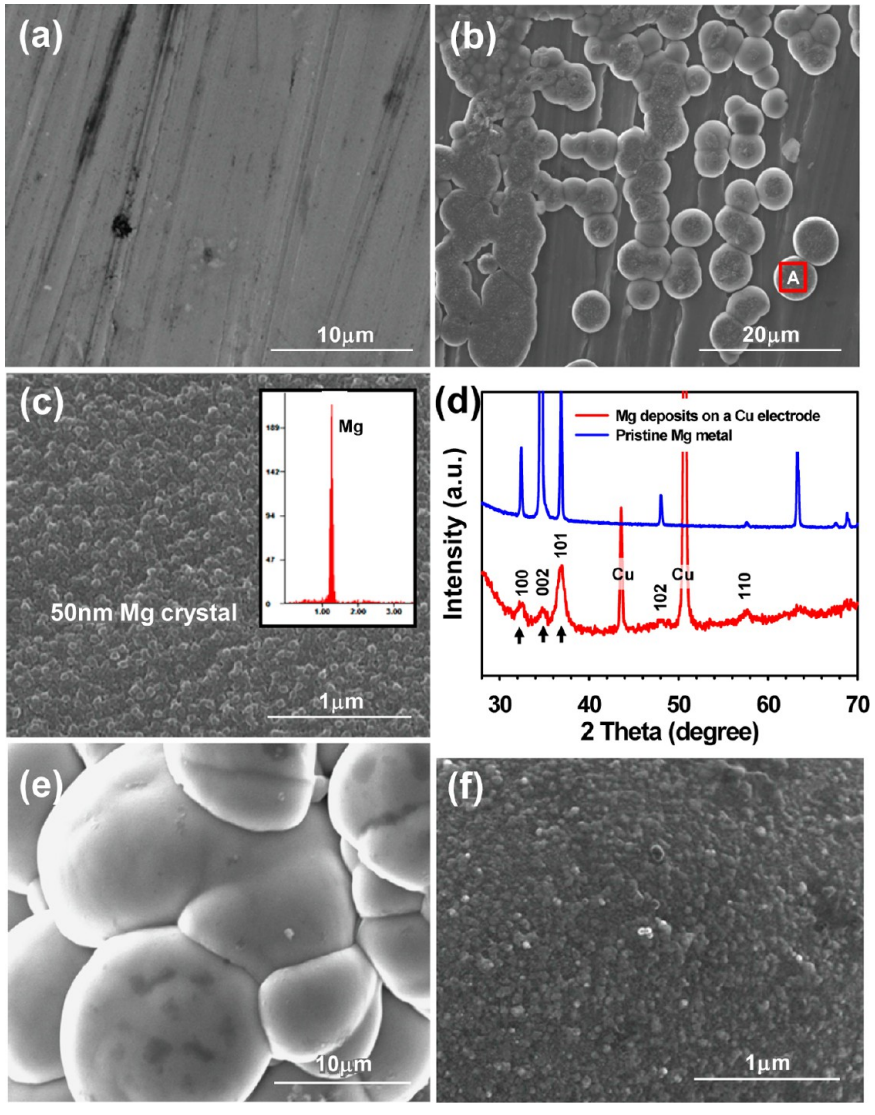

Figure 6. (a) SEM image of pristine Mg electrode. (b) SEM image of Mg electrode after first Mg deposition at a rate of 1C (3.25 mA/cm^2). The SEM images reveal that nondendritic Mg deposits are formed on the Mg electrode surface even at a high rate of 1C (3.25 mA/cm^2). (c) SEM image of a selected zone A of b. The inset shows the EDS spectrum of Mg deposits without the signal from the electrolyte decomposition. (d) XRD pattern of the galvanostatic deposition of Mg on a Cu electrode at a rate of C/5 (1.3 mA/cm^2) in glyme/diglyme (1/1, v/v) with 0.3 M Mg(TFSI)$_2$. (e) SEM image of Mg deposits on a Cu electrode. (f) Magnified SEM image of e.

exhibited a relatively low initial potential drop of −0.354 V during the first Mg stripping compared to 0.3 M Mg(TFSI)$_2$ in glyme/diglyme (initial overpotential ≈ −2.0 V) (Figure 3e and Figures S6c and S7a in the Supporting Information). The ICP

dx.doi.org/10.1021/am405619v | ACS Appl. Mater. Interfaces 2014, 6, 4063−4073

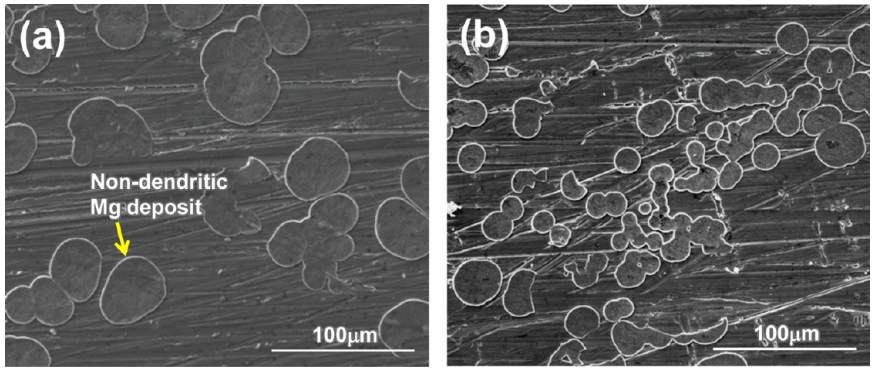

Figure 7. (a) SEM image of the Mg electrode after first cathodic scan at the current density of 0.163 mA/cm^2 (corresponding capacity = 3.25 mAh/cm^2). (b) SEM image of the Mg electrode after first cathodic scan at the current density of 0.65 mA/cm^2 (corresponding capacity = 3.25 mAh/cm^2).

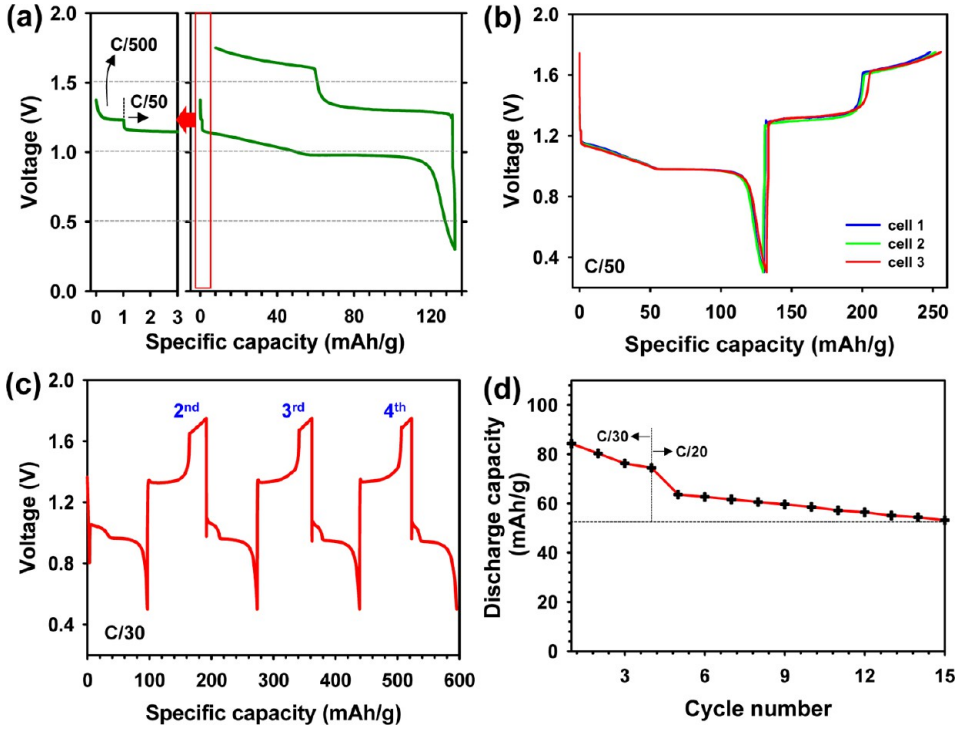

Figure 8. (a) First discharge and charge curves of the Mg/Mo_6S_8 cell at a rate of $C/50$ between 0.3 and 1.75 V. The left plot displays that a very low rate of $C/500$ was applied to cells during 5 h of the first discharge and was then increased to $C/50$. (b) Cycling performance of the Mg/Mo_6S_8 cell at a rate of $C/30$. (c) Discharge and charge profiles of the Mg/Mo_6S_8 cell at a rate of $C/30$ between 0.5 and 1.75 V. (d) Cycling property of the Mg/Mo_6S_8 cell after the first 2 cycles at $C/30$ and $C/20$.

result reveals that 665 ppm of Mg from MgO is dissolved in 0.4 M $(PhMgCl)_2$-$AlCl_3$/THF electrolyte for 1 h. This result implies that the 0.4 M $(PhMgCl)_2$-$AlCl_3$/THF electrolyte readily removes the surface oxide layer from the Mg electrode because of its superior ability to dissolve an oxide layer and effectively initiates the Mg stripping/deposition.

Clearly, once Mg dissolution from the Mg electrode is initiated, further Mg stripping at the Mg electrode and Mg deposition at the Cu electrode readily take place without a significant potential barrier. After this activation process, no large overpotential in diglyme with 0.1 M $Mg(TFSI)_2$ appeared again during cycling (see Figure S7b in the Supporting Information). The potential change for Mg stripping and deposition in Mg/Mg symmetrical cells with 0.3 M $Mg(TFSI)_2$ dissolved in diglyme or a glyme/diglyme mixture was investigated for various current densities of 0.25, 0.375, 0.75, and 1.5 mA/cm^2.

Stable potential profiles between the two Mg electrodes were clearly observed in the subsequent cycling for current densities of 0.25 mA/cm^2 and 0.375 mA/cm^2, and the corresponding overpotential profiles increased slightly with increasing current density (Figure 4f). By contrast, diglyme with 0.3 M $Mg(TFSI)_2$ showed a high potential barrier and led to a significant increase in the overpotential (i.e., ΔV) with increasing current density. This result is in agreement with Table 2, which shows the effect of solvent species on ionic conductivities. From the rate capability results and solubility tests of Mg salt, it is believed that $Mg(TFSI)_2$ is primarily dissociated by diglyme and that glyme is entirely responsible for providing a low viscous conduction medium in glyme/diglyme-based electrolytes.

3.3. Mg Crystal Formed in $Mg(TFSI)_2$-Based Electrolytes. Figures 6b, c and 7a, b show SEM images of nondendritic Mg deposits on a Mg electrode obtained at

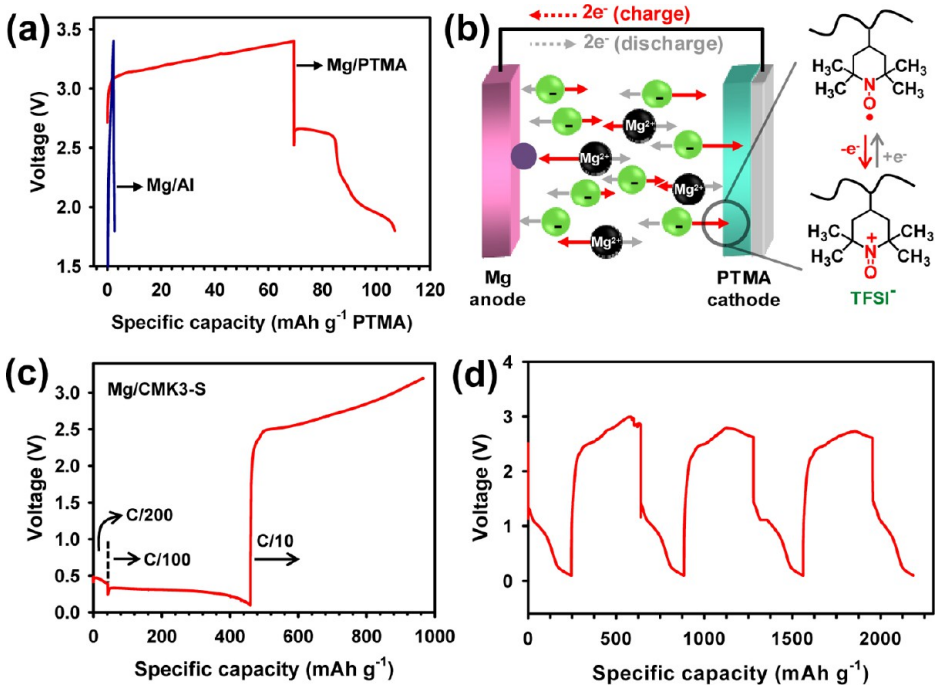

Figure 9. (a) First charge (Mg plating on a Mg anode) and discharge (Mg stripping from a Mg anode) curves of Mg/PTMA and Mg/aluminum cells, (b) Schematic of electrochemical oxidation and reduction of the PTMA cathode in an Mg/PTMA cell, (c) First discharge and charge of an Mg/CMK3-S cell, and (d) galvanostatic cycling of an Mg/CMK3-S cell from 1 to 4 cycles at a rate of C/50 after activation cycles.

0.163, 0.65, and 3.25 mA/cm^2. This result agrees well with previous results.[7] Nondendritic Mg deposits were formed in glyme/diglyme with 0.3 M $Mg(TFSI)_2$, even at a high current density of 3.25 mA/cm^2 (Figure 6b, c). It is notable that agglomerated Mg secondary particles composed of approximately 50 nm primary particles were observed on the electrochemically deposited Mg particles obtained from glyme/diglyme with 0.3 M $Mg(TFSI)_2$, as shown in the magnified SEM image (Figure 6c, f). The nanosized agglomerated morphology produces relatively high surface area on the Mg electrodes, and this appears to result in high electrochemical activity (low polarization) for Mg stripping. This morphology is further supported by the broader XRD peaks (larger fwhm) of the electrochemically deposited Mg on a Cu electrode relative to the peaks of the pristine Mg metal (Figure 6d, e). Moreover, only elemental Mg was observed in the deposited Mg particles, as shown in the EDS spectrum (inset of Figure 6c), indicating that no electrolyte decomposition occurs during Mg deposition on the Mg electrode.

3.4. Battery Performance in $Mg(TFSI)_2$-Based Electrolytes. To demonstrate that glyme/diglyme with 0.3 M $Mg(TFSI)_2$ allows magnesiation/demagnesiation of Mo_6S_8 in a Mg-ion battery, the cycling properties of Mg/Mo_6S_8 cells were investigated, as shown in Figure 8a. The first discharge and charge capacities of a Mg/Mo_6S_8 cell (the theoretical capacity of Mo_6S_8 is 128.8 mAh/g) with glyme/diglyme/0.3 M $Mg(TFSI)_2$ were 132 mAh/g and 125 mAh/g, respectively (Figure 8a). The excellent Mg extraction capacity of 125 mAh/g is ascribed to its slow C rate, providing sufficient demagnesiation of Mo_6S_8. A Mg/Mo_6S_8 cell with glyme/diglyme/0.3 M $Mg(TFSI)_2$ delivers a reversible capacity of ca. 97 mAh/g at the second cycle (Figure 8b). Moreover, reversible cycling performance was shown in the glyme/diglyme/0.3 M $Mg(TFSI)_2$ electrolyte during further cycling at a rate of C/30 (Figure 8c). Nevertheless, the gradual capacity fading that accompanies each charge and discharge is displayed at a rate of C/20, as shown in Figure 8b. This behavior is most likely because the sluggish kinetics of the glyme/diglyme/0.3 M $Mg(TFSI)_2$ electrolyte impedes the Mg insertion into the inner site of Mo_6S_8 at approximately 1.0 V vs Mg/Mg^{2+}.

To confirm the oxidative stability of 0.3 M $Mg(TFSI)_2$ in glyme/diglyme at a high voltage cathode, galvanostatic cycling for a Mg/PTMA (theoretical capacity = 111 mAh/g) cell was performed, as presented in Figure 9a.[28] To overcome the initial potential barrier for Mg stripping at the Mg anode, the discharge process was conducted at a low rate of C/50. The cell showed capacities of 69.4 mAh/g and 37.6 mAh/g for the first charge and discharge processes (Figure 9a,b), respectively. In addition, when the Mg/Al cell was charged to 3.4 V, discernible charge and discharge capacities were not observed. This result indicates that there is no corrosion of the Al current collector in 0.3 M $Mg(TFSI)_2$ in glyme/diglyme. Very recently, a significant advancement in the research on Mg battery electrolytes was shown by the Toyota research group.[13] They reported that hexamethyl-disilazane magnesium chloride was compatible with a Mg/sulfur (S) cell. A solution of 0.3 M $Mg(TFSI)_2$ in glyme/diglyme was used as an electrolyte to investigate its compatibility with a S cathode. To overcome the initial overpotential for the initiation of Mg stripping in Mg/CMK3-S cells, a very slow rate of C/200 was applied to the cells for 5 h of the first discharge. The applied rate was then increased to C/100 at the first discharge, and the rate for the first charge was C/10 (Figure 9c). The Mg/CMK3-S cell with 0.3 M $Mg(TFSI)_2$ in glyme/diglyme exhibited a discharge capacity of 500 mAh g^{-1} and a potential plateau of 0.2 V. This result indicates that magnesium sulfide (MgS) is reversibly formed, which is supported by the XRD results. Figure S8 in the Supporting Information shows that a peak corresponding to MgS was formed at the first discharge, and its peak intensity was slightly reduced after the first charge. It should be noted

dx.doi.org/10.1021/am405619v | ACS Appl. Mater. Interfaces 2014, 6, 4063−4073

that the well-resolved peaks corresponding to bulk crystalline sulfur completely disappear after sulfur is impregnated in CMK-3.[29] Although the electrochemical conversion of sulfur to MgS in a Mg/CMK3-S cell takes place successfully in 0.3 M $Mg(TFSI)_2$ in glyme/diglyme, the shuttle process, mainly by the dissolution of long chain polysulfide anions (S_n^{2-}) into the electrolyte, was not completely eliminated (Figure 9d). Although some electrolytes such as magnesium organohaloaluminate with a formula of $Mg(AlCl_2BuEt)_2$ have shown impressive electrochemical properties in Mg batteries coupled with Chevrel phase Mo_6S_8 insertion cathodes, they were found to be corrosive toward the current collectors and showed low anionic stability against high voltage. A high energy density in Mg batteries can be achieved by increasing the discharge capacity of the cathode or by augmenting the working potential of the cathode materials. Hence, the discovery of Mg electrolytes with a wide electrochemical stability is vital for achieving a rechargeable Mg battery with high energy density. Glyme/digylme with $Mg(TFSI)_2$ showed superior anodic stability, a highly reduced corrosive nature toward SS and Al electrodes, and excellent compatibility with high voltage cathodes, PTMA, and CMK-3/S composite. Surprisingly, Mg has been successfully deposited from glyme/diglyme/Mg-$(TFSI)_2$ without an ion-blocking layer, indicating that electrolyte decomposition did not occur on the Mg electrode (inset of Figure 6c: EDS spectrum of Mg deposits). Furthermore, the excellent oxidation durability of glyme/diglyme/$Mg(TFSI)_2$ is expected to stimulate the development of high voltage cathodes of more than 2.0 V versus Mg/Mg^{2+}. Although the electrochemical oxidation and reduction of a high voltage PTMA cathode occurs in glyme/digylme with $Mg(TFSI)_2$, capacity fading appeared at the second cycle because of the partial solubility of PTMA in the electrolyte.

This challenge could be overcome by reducing the solubility of the molecular architecture of the electrochemically active radical polymer in the electrolytes. The inset of Figure 9d presents the excellent discharge capacity retention of a Mg/CMK3-S cell from the first to fourth cycles at a rate of C/50 after activation cycling. However, the charge and discharge curves of Figure 9d reveal that Mg/CMK3-S cells with glyme/diglyme/$Mg(TFSI)_2$ still suffer from the shuttle phenomenon due to the high solubility of polysulfides. Promising approaches such as surface coating using poly(3,4-ethylenedioxythiophene)-poly(styrenesulfonate) (PEDOT:PSS) to confine polysulfides more effectively have been reported.[27] It is expected that further modification of a CMK-3 mesoporous carbon/sulfur composite cathode would mitigate the shuttle mechanism.

4. CONCLUSIONS

We have demonstrated for the first time a unique and extremely promising electrolyte based on glymes with $Mg(TFSI)_2$ for rechargeable Mg batteries. $Mg(TFSI)_2$ dissolved in glyme/diglyme showed excellent anodic stability exceeding 4.0 V with Al used as a cathode current collector, which is impossible in organohaloaluminate Mg salt-based electrolytes. In addition, galvanostatic cycling tests of Mg/Mg and Mg/Cu cells confirmed that glyme/diglyme with $Mg(TFSI)_2$ has sufficient solvating power to initiate Mg stripping at the Mg electrode, and the large potential barrier for Mg stripping does not reappear during further cycling. Furthermore, it was found that a glyme-$Mg(TFSI)_2$ salt complex allows the electrochemical oxidation and reduction of a Chevrel phase Mo_6S_8 insertion cathode, a pendant radical polymer with a robust 2,2,6,6-tetramethyl-piperidinyl-*N*-oxy (TEMPO) radical moiety charged to a high voltage of 3.4 V versus Mg/Mg^{2+} and a carbon−sulfur (CMK-3/S) composite cathode. We hope that the results of this study and the associated analysis will contribute to the search for a whole new class of cathodes with the promise of further improvement in the electrochemical performance of rechargeable Mg batteries.

■ ASSOCIATED CONTENT

Supporting Information

More characterization results. This material is available free of charge via the Internet at http://pubs.acs.org.

■ AUTHOR INFORMATION

Corresponding Authors

*E-mail: ktlee@unist.ac.kr.
*E-mail: nschoi@unist.ac.kr.

Notes

The authors declare no competing financial interest.

■ ACKNOWLEDGMENTS

This work was supported by the IT R&D program of MOTIE/KEIT(KI001810046309) and by a grant from the Energy Efficiency & Resources of the Korea Institute of Energy Technology Evaluation and Planning(Project no. 20112010100140) funded by the Korean Ministry of Knowledge Economy.

■ REFERENCES

(1) Etacheri, V.; Marom, R.; Elazari, R.; Salitra, G.; Aurbach, D. Challenges in The Development of Advanced Li-Ion Batteries: A Review. *Energy Environ. Sci.* **2011**, *4*, 3243−3262.
(2) Wu, H.; Cui, Y. Designing Nanostructured Si Anodes for High Energy Lithium Ion Batteries. *Nano Today* **2012**, *7*, 414−429.
(3) Dunn, B.; Kamath, H.; Tarascon, J. M. Electrical Energy Storage for the Grid: A Battery of Choices. *Science* **2011**, *334*, 928−935.
(4) Choi, N. -S.; Chen, Z. H.; Freunberger, S. A.; Ji, X. L.; Sun, Y. K.; Amine, K.; Yushin, G.; Nazar, L. F.; Cho, J.; Bruce, P. G. Challenges Facing Lithium Batteries and Electrical Double-Layer Capacitors. *Angew. Chem.-Int. Edit.* **2012**, *51*, 9994−10024.
(5) Aurbach, D.; Lu, Z.; Schechter, A.; Gofer, Y.; Gizbar, H.; Turgeman, R.; Cohen, Y.; Moshkovich, M.; Levi, E. Prototype Systems for Rechargeable Magnesium Batteries. *Nature* **2000**, *407*, 724−727.
(6) Yoo, H. D.; Shterenberg, I.; Gofer, Y.; Gershinsky, G.; Pour, N.; Aurbach, D. Mg Rechargeable Batteries: An On-going Challenge. *Energy Environ. Sci.* **2013**, *6*, 2265−2279.
(7) Matsui, M. Study on Electrochemically Deposited Mg Metal. *J. Power Sources* **2011**, *196*, 7048−7055.
(8) Kumar, Y.; Hashmi, S. A.; Pandey, G. P. Ionic Liquid Mediated Magnesium Ion Conduction in Poly(ethylene oxide) Based Polymer Electrolyte. *Electrochim. Acta* **2011**, *56*, 3864−3873.
(9) Levi, E.; Gofer, Y.; Aurbach, D. On the Way to Rechargeable Mg Batteries: The Challenge of New Cathode Materials. *Chem. Mater.* **2010**, *22*, 860−868.
(10) Wang, F. F.; Guo, Y. S.; Yang, J.; Nuli, Y.; Hirano, S. A Novel Electrolyte System without a Grignard Reagent for Rechargeable Magnesium Batteries. *Chem. Commun.* **2012**, *48*, 10763−10765.
(11) Muldoon, J.; Bucur, C. B.; Oliver, A. G.; Sugimoto, T.; Matsui, M.; Kim, H. S.; Allred, G. D.; Zajicek, J.; Kotani, Y. Electrolyte Roadblocks to a Magnesium Rechargeable Battery. *Energy Environ. Sci.* **2012**, *5*, 5941−5950.
(12) Mohtadi, R.; Matsui, M.; Arthur, T. S.; Hwang, S. J. Magnesium Borohydride: From Hydrogen Storage to Magnesium Battery. *Angew. Chem., Int. Ed.* **2012**, *51*, 9780−9783.

(13) Kim, H. S.; Arthur, T. S.; Allred, G. D.; Zajicek, J.; Newman, J. G.; Rodnyansky, A. E.; Oliver, A. G.; Boggess, W. C.; Muldoon, J. Structure and Compatibility of a Magnesium Electrolyte with a Sulphur Cathode. *Nat. Commun.* **2011**, *2*, 427.
(14) Aurbach, D.; Gizbar, H.; Schechter, A.; Chusid, O.; Gottlieb, H. E.; Gofer, Y.; Goldberg, I. Electrolyte Solutions for Rechargeable Magnesium Batteries Based on Organomagnesium Chloroaluminate Complexes. *J. Electrochem. Soc.* **2002**, *149*, A115−A121.
(15) Lv, D. P.; Xu, T.; Saha, P.; Datta, M. K.; Gordin, M. L.; Manivannan, A.; Kumta, P. N.; Wang, D. H. A Scientific Study of Current Collectors for Mg Batteries in $Mg(AlCl_2EtBu)_2$/THF Electrolyte. *J. Electrochem. Soc.* **2013**, *160*, A351−A355.
(16) Lu, Z.; Schechter, A.; Moshkovich, M.; Aurbach, D. On the Electrochemical Behavior of Magnesium Electrodes in Polar Aprotic Electrolyte Solutions. *J. Electroanal. Chem.* **1999**, *466*, 203−217.
(17) Doe, R. E.; Han, R.; Hwang, J.; Gmitter, A. J.; Shterenberg, I.; Yoo, H. D.; Pour, N.; Aurbach, D. Novel, Electrolyte Solutions Comprising Fully Inorganic Salts with High Anodic Stability for Rechargeable Magnesium Batteries. *Chem. Commun.* **2014**, *50*, 243−245.
(18) Liao, C.; Guo, B.; Jiang, D.; Custelcean, R.; Mahurin, S. M.; Sun, X.-G.; Dai, S. Highly Soluble Alkoxide Magnesium Salts for Rechargeable Magnesium Batteries. *J. Mater. Chem. A* **2014**, DOI: 10.1039/C3TA13691D.
(19) Singh, N.; Arthur, T. S.; Ling, C.; Matsui, M.; Mizuno, F. A High Energy-density Tin Anode for Rechargeable Magnesium-Ion Batteries. *Chem. Commun.* **2013**, *49*, 149−151.
(20) Tran, T. T.; Lamanna, W. M.; Obrovac, M. N. Evaluation of $Mg[N(SO_2CF_3)_2]_2$/Acetonitrile Electrolyte for Use in Mg-Ion Cells. *J. Electrochem. Soc.* **2012**, *159*, A2005−A2009.
(21) Pour, N.; Gofer, Y.; Major, D. T.; Aurbach, D. Structural Analysis of Electrolyte Solutions for Rechargeable Mg Batteries by Stereoscopic Means and DFT Calculations. *J. Am. Chem. Soc.* **2011**, *133*, 6270−6278.
(22) Chusid, O.; Gofer, Y.; Gizbar, H.; Vestfrid, Y.; Levi, E.; Aurbach, D. Solid-State Rechargeable Magnesium Batteries. *Adv. Mater.* **2003**, *15*, 627−630.
(23) Lin, C. H.; Chau, C. M.; Lee, J. T. Synthesis and Characterization of Polythiophene Grafted with a Nitroxide Radical Polymer via Atom Transfer Radical Polymerization. *Polym. Chem.* **2012**, *3*, 1467−1474.
(24) Ji, X. L.; Lee, K. T.; Nazar, L. F. A Highly Ordered Nanostructured Carbon-Sulphur Cathode for Lithium-Sulphur Batteries. *Nat. Mater.* **2009**, *8*, 500−506.
(25) Kühnel, R.-S.; Lübke, M.; Winter, M.; Passerini, S.; Balducci, A. Suppression of Aluminum Current Collector Corrosion in Ionic Liquid Containing Electrolytes. *J. Power Sources* **2012**, *214*, 178−184.
(26) Gizbar, H..; Vestfrid, Y.; Chusid, O.; Gofer, Y.; Gottlieb, H. E.; Marks, V.; Aurbach, D. Alkyl Group Transmetalation Reactions in Electrolytic Solutions studied by Multinuclear NMR. *Organometallics* **2004**, *23*, 3826−3831.
(27) Laoire, C. O.; Mukerjee, S.; Plichta, E. J.; Hendrickson, M. A.; Abraham, K. M. Rechargeable Lithium/TEGDME-$LiPF_6$/O_2 Battery. *J. Electrochem. Soc.* **2011**, *158*, A302−A308.
(28) Nakahara, K.; Iwasa, S.; Satoh, M.; Morioka, Y.; Iriyama, J.; Suguro, M.; Hasegawa, E. Rechargeable Batteries with Organic Radical Cathodes. *Chem. Phys. Lett.* **2002**, *359*, 351−354.
(29) Yang, Y.; Yu, G. H.; Cha, J. J.; Wu, H.; Vosgueritchian, M.; Yao, Y.; Bao, Z. A.; Cui, Y. Improving the Performance of Lithium-Sulfur Batteries by Conductive Polymer Coating. *ACS Nano* **2011**, *5*, 9187−9193.